AIP | The Journal of Chemical Physics

Molecular dynamics investigation of desorption and ion separation following picosecond infrared laser (PIRL) ablation of an ionic aqueous protein solution

J. Zou, C. Wu, W. D. Robertson, L. V. Zhigilei, and R. J. D. Miller

Citation: The Journal of Chemical Physics **145**, 204202 (2016); doi: 10.1063/1.4967164
View online: http://dx.doi.org/10.1063/1.4967164
View Table of Contents: http://scitation.aip.org/content/aip/journal/jcp/145/20?ver=pdfcov
Published by the AIP Publishing

Molecular dynamics investigation of desorption and ion separation following picosecond infrared laser (PIRL) ablation of an ionic aqueous protein solution

J. Zou,[1] C. Wu,[2] W. D. Robertson,[3] L. V. Zhigilei,[2] and R. J. D. Miller[1,3,a)]
[1]*Departments of Chemistry and Physics, University of Toronto, 80 St. George Street, Toronto, Ontario M5S 3H6, Canada*
[2]*Department of Materials Science and Engineering, University of Virginia, Charlottesville, Virginia 22904-4745, USA*
[3]*Max Plank Institute for the Structure and Dynamics of Matter, 149 Luruper Chaussee, 27761 Hamburg, Germany*

(Received 18 July 2016; accepted 3 October 2016; published online 30 November 2016)

Molecular dynamics simulations were performed to characterize the ablation process induced by a picosecond infrared laser (PIRL) operating in the regime of desorption by impulsive vibrational excitation (DIVE) of a model peptide (lysozyme)/counter-ion system in aqueous solution. The simulations were performed for ablation under typical experimental conditions found within a time-of-flight mass spectrometer (TOF-MS), that is in vacuum with an applied electric field ($E = \pm 10^7$ V/m), for up to 2 ns post-ablation and compared to the standard PIRL-DIVE ablation condition (E = 0 V/m). Further, a simulation of ablation under an extreme field condition ($E = 10^{10}$ V/m) was performed for comparison to extend the effective dynamic range of the effect of the field on charge separation. The results show that the plume dynamics were retained under a typical TOF-MS condition within the first 1 ns of ablation. Efficient desorption was observed with more than 90% of water molecules interacting with lysozyme stripped off within 1 ns post-ablation. The processes of ablation and desolvation of analytes were shown to be independent of the applied electric field and thus decoupled from the ion separation process. Unlike under the extreme field conditions, the electric field inside a typical TOF-MS was shown to modify the ions' motion over a longer time and in a soft manner with no enhancement to fragmentation observed as compared to the standard PIRL-DIVE. The study indicates that the PIRL-DIVE ablation mechanism could be used as a new, intrinsically versatile, and highly sensitive ion source for quantitative mass spectrometry. *Published by AIP Publishing.* [http://dx.doi.org/10.1063/1.4967164]

I. INTRODUCTION

Rapid advances in proteomics, lipidomics, metabolomics, and other protein and biomolecule based fields have driven the ever increasing demand for quantitative analytical methods with high sensitivity. Mass spectrometry (MS) has been widely utilized in biological research following the development of matrix-assisted laser desorption/ionization (MALDI)[1] and electrospray ionization (ESI),[2] which have allowed for the gas phase production of large labile protein ions for MS analysis. Currently, commercially available mass-spectrometry-based systems are capable of identifying a wide variety of biomolecules, with femto- and attomole detection limits being commonplace and even 30 zeptomole (~18 000 molecules) being recently reported with a combination of ESI and a Fourier Transform Ion Cyclotron Resonance (FT-ICR) mass analyzer.[3] The rapid improvement in the performance of ion sources and mass analyzers has led to enhanced sensitivity and mass resolution. However, inherent limitations of current ion source technology continue to result in ionization efficiencies differing significantly for various analytes and sample conditions with MS remaining predominantly qualitative in nature.[4]

Electrospray ionization (ESI), the method commonly utilized for proteomic investigation due to the highly charged species readily produced, has an efficiency that is molecule dependent and greatly deteriorated by the presence of additives, such as other analytes or salts.[3,4] Therefore, appropriate sample purification procedures are essential prior to analysis. The laser based MALDI technique has been widely used for analyzing medium to high molecular weight molecules with limits of detection in the femtomole and occasionally the attomole range achieved for many biological analytes such as metabolites, lipids, peptides, and proteins.[1,5] The method typically results in singly charged species and is considered less soft than ESI. Numerous MALDI matrices, which introduce spectral artifacts, are available and required for specific molecule types. The sensitivity of MALDI-MS depends heavily on the matrix, as well as on the sample preparation and the quality of the sample/matrix layer. Neither ESI nor MALDI based methods have been successful as a versatile ion source to directly analyze complex samples composed of multiple types of molecules over a wide molecular weight and concentration range. For most

a)dmiller@lphys.chem.utoronto.ca

ion sources utilized today, complex sample preparation is required in order to extract known molecules of interest for analysis from complex biological samples. These sample preparation procedures can be intricate and specific for each type of molecule, instrument, and ionization source with each laboratory producing its own unique recipe and results.[6] This significantly reduces the applicability of MS even though high sensitivity can be achieved. In order to utilize MS for quantitative analysis and eliminate the need for analyte specific sample preparations, a versatile analyte extraction and ionization source is needed, which is free of the limitations associated with ESI and MALDI.

Recently, an ablation process utilizing a novel picosecond infrared laser desorption via impulsive vibrational excitation (PIRL-DIVE) has provided a promising mechanism for the development of such an ion source.[7] In PIRL-DIVE, the photon energy of the laser pulse is selectively deposited into the OH vibrational stretch mode of water molecules. The OH stretch mode of water is directly coupled through the water hydrogen bond network to the O–O translation motion, the very motion needed to drive ablation.[8] The deposited energy is transferred into translational motion on a time scale that is faster than the thermal and acoustic energy redistribution.[8] IR laser ablation with similar wavelength but longer pulse duration has been demonstrated using Er:YAG lasers (pulse duration 100 ns–100 μs) and with Nd:YAG pumped optical parametric oscillator (pulse duration ~10 ns). The ablation induced by longer laser pulses has been successfully coupled with secondary post-ionization sources, such as electrospray in Laser Ablation Electrospray Ionization (LAESI), for direct MS analysis of biological samples.[9,10] The slower energy deposition process allows the deposited energy to be transferred into the analyte molecules and to penetrate into the surrounding tissue, resulting in the tissue and analyte damage.[11] The rapid energy deposition process of PIRL-DIVE allows the ablated water molecules to act as a propellant to drive the analyte molecules, such as proteins dissolved in water, into the gas phase in an intact and cold manner. These undamaged gas phase molecules are then available for ionization and MS analysis. To date, all PIRL-DIVE characterization studies have been performed under atmospheric conditions where efficient extraction of water rich biological materials has been demonstrated.[11–13] This method is not restricted to aqueous solution but is also readily applicable to biological tissue where the water content can be as high as 60%-70% and has even been shown to be very effective in low water content tissue such as dentin.[12] This application allows direct spatial mapping of tissue with MS without any specialized matrix. Further, the application of PIRL-DIVE to numerous surgical scenarios has demonstrated that the technique produces minimal tissue damage outside the ablation zone and minimizes scar tissue formation.[11,14] Moreover, the ultra-soft nature of the process is evident by the retention of native enzymatic activity and viral infectivity of species collected from the plume of PIRL-DIVE ablated materials.[15,16] In aqueous solution and cellular environments, proteins and other biological molecules are typically charged via protonation or adduct formation with associated counter-ions present in the vicinity to balance the charge. This initial state makes it possible to utilize DIVE to effectively desorb charged biomolecular ions directly into the gas phase. Recently we have applied PIRL-DIVE as a new ambient ion source for mass spectrometry imaging in combination with ESI, so-called picosecond infrared laser ablation electrospray ionization (PIR-LAESI).[17] PIR-LAESI has demonstrated the capability of ionizing a wide range of molecules including small drugs, lipids, and proteins, with a limit of detection of 25 fmol for reserpine extracted from agarose gel. PIR-LAESI has been successfully applied to map the distribution of endogenous methoxykaempferol glucoronide in zebra plant (Aphelandra squarrosa) leaves and the distribution of gadoteridol, an exogenous magnetic resonance contrast agent, intravenously injected into mouse kidney.[17]

We have previously studied the plume dynamics of PIRL-DIVE ablation applied to pure liquid water under atmospheric conditions using Euler hydrodynamics numerical simulations applied within the Lagrangian framework.[7] The simulations showed that the ablated water volume expands at a speed of 1500 m/s within the first 1 ns after laser irradiation with the temperature of the plume reaching approximately 1200 K. However, the fluid dynamics model can only provide general information on the plume characteristics. In order to gain further insight into the ablation physics, including the microscopic mechanisms of water desorption and separation of counter-ions from analytes within the ablation plume, a more robust, molecular level method is needed. Molecular dynamics (MD) simulations have been heavily utilized to investigate physical phenomena involved in the complex processes during laser ablation. The ablation plume dynamics, including the evolution of temperature, pressure, and plume composition (single molecule/aggregates/clusters, etc.), have been characterized.[18–24] Moreover, MD simulations have been successfully applied to study the ionization mechanisms in MALDI and to elucidate the parameters that affect ion yield.[25,26]

Here, MD simulations were employed to evaluate DIVE as a direct biomolecular ion source by modeling PIRL-DIVE ablation of a thin film of aqueous solution containing a lysozyme based peptide/counter-ion model system to mimic the experimental conditions. The simulation is performed in vacuum, as typical for time-of-flight (TOF) mass spectrometry, with a sample peptide concentration analogous to that found in cellular environments (8.3 mM).[27] The model was used to investigate the ability of PIRL-DIVE ablation to strip away water and counter-ions from charged proteins leaving them directly available for mass analysis. Further, we assess the effect of a MS electric field on charged protein/counter-ion separation, as a further indication of the feasibility of the method as a soft, quantitative ion source. The results reveal that the plume dynamics is retained under typical TOF-MS conditions with efficient water desorption from the lysozyme chains observed. Up to 90% of water molecules interacting with the peptide was stripped away in the first nanosecond of the ablation plume expansion. Ablation plume expansion is shown to dominate the ions' motion within the first 1 ns, with the desorption process being independent of the applied electric field and decoupled from the ion separation process. Protein-counterion separation induced by the electric field was observed in the late stages of

ablation and it was further revealed that the electric field strength of a typical TOF-MS promotes charge separation in a soft manner without enhanced peptide fragmentation. These results indicate that PIRL-DIVE is a feasible method for the development of an intrinsically versatile and highly sensitive new concept ion source for quantitative mass spectrometry. As the ablation mechanism is in principle independent of molecular and solution properties, the technique has a general appeal as a novel ion source requiring no sample preparation.

II. MD SIMULATION MODEL

The MD simulations were performed to model the laser ablation of a thin film of peptide/counter-ion system. A conceptual scheme of the simulated scenario is shown in Fig. 1, with the protein molecule shown in green, and a bound salt ion, a counter-ion, and water molecules are represented as blue, yellow, and red particles, respectively. The PIRL irradiation, propagating from the left through the transparent conductive plate, has a wavelength of 2.94 μm, an incident fluence of 1 J/cm^2, and a Gaussian temporal profile with the full width at half-maximum (FWHM) of 100 ps. These parameters were selected to simulate DIVE conditions, as previously demonstrated in experimental studies.[17] The system used in the simulations is a 70 nm thick film of an aqueous solution of lysozyme molecules deposited on a transparent conductive plate, through which the laser is directed. The thickness of the film is much smaller than the PIRL optical penetration depth of water (~2 μm) leading to a homogeneous excitation of the entire sample volume. Experimentally, this setup can be used for films that are thinner than the optical penetration depth, while for thicker films the ablation can be induced through irradiation from the opposite direction. An external electric field was applied between two parallel electrodes (Fig. 1) as is typical for TOF-MS. For simplicity, each lysozyme chain was assumed to be attached to a singly charged (e^+) salt ion while one of the surrounding matrix molecules is assigned a single negative charge (e^-) to serve as the counter-ion, resulting in an overall neutral system. In order to mimic experimental conditions within a TOF-MS (Fig. 1), the simulation was performed for ablation in vacuum under typical MS electric field values, E = $\pm 10^7$ V/m. Here, the negative sign "–" describes

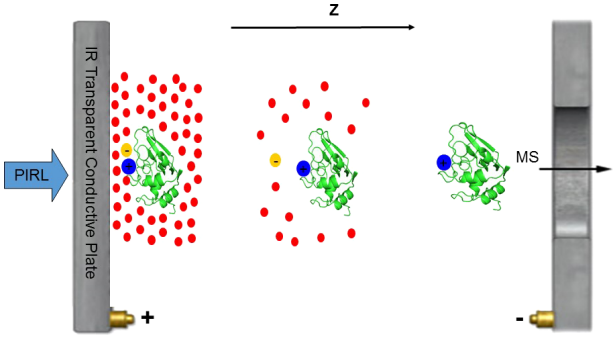

FIG. 1. Conceptual scheme of PIRL-DIVE ablation of ionic aqueous protein solution under external electric field.

an electric field acting to decelerate the ablated positively charged lysozyme molecules. In order to compare the effect of the electric field on the plume properties and lysozyme-counter-ion separation, simulations were also performed for the ablation with E = 0 V/m as well as with a very large electric field, E = 10^{10} V/m. The very large electric field enabled an effective observation of the field action on the ion distribution that would take much longer to simulate at lower field and provided a simple means to artificially extend the dynamic range of this study. Following laser irradiation, the simulations were performed for 2 ns for fields of 0 V/m and 10^7 V/m and 1 ns for fields of 10^{10} V/m and -10^7 V/m.

The direct application of the conventional all-atom MD representation of the aqueous protein solution in large-scale simulations of laser ablation is not feasible due to the high computational cost. Thus, a coarse-grained representation of both water matrix and lysozyme molecules is adapted in the current study. The coarse-grained MD model combines the breathing sphere (BS) model developed for simulations of molecular systems[20,24,28] with the bead-and-spring model commonly used in modeling of polymers.[24,29] The technical details of the coarse-grained model can be found in a recent paper,[30] and only the main points related to the present simulations are briefly outlined below.

In the coarse-grained model, the dynamic unit is a spherical particle that represents a molecular group that is void of any intramolecular structure. The spherical particle has a mass M and radius R undergoing breathing vibrations, i.e., expanding or contracting around an equilibrium radius R_0. In the water-lysozyme system, a breathing sphere represents a group of water molecules or a monomer in a lysozyme chain, that is, a bead in the bead-and-spring model representation. Each BS particle of water is assigned a mass of M = 50 Da, representing ~3 water molecules as a unit. Each lysozyme chain is made up of 129 monomer units (beads), whereas each bead represents an amino acid residue of chicken egg-white lysozyme[30] with a mass of M = 111 Da (14 307 Da/129 ≈ 111 Da). The breathing motion is controlled by an inertia parameter (or effective mass) M_I ascribed to the corresponding breathing degree of freedom and an anharmonic potential,[28,30]

$$U_R(R_i) = k_1(R_i - R_0)^2 + k_2(R_i - R_0)^3 + k_3(R_i - R_0)^4, \quad (1)$$

where k_1, k_2 and k_3 are parameters of the potential and R_i is an instantaneous value of radius R of a BS particle i.

The breathing motions are coupled with the translational motions of the spherical particles, which are described by the Morse potential $U_r(r_{ij}^S)$[31–33] defined as a function of the distance between edges of two breathing sphere particles i and j, r_{ij}^S. The coupling strength is controlled by the parameters M_I, k_1, k_2 and k_3. The choice of the parameters, therefore, can be used to ensure that the rate of the energy equilibration between the optically excited molecules and their surroundings matches the results of pump-probe experiments or atomistic simulations.[23,28,30] The parameters of the internal potential given by Eq. (1) are listed for the water and lysozyme units of the coarse-grained model in Table I. These parameters

TABLE I. Parameters of the internal potential for water and lysozyme components of the coarse-grained model.

	M_I, Da	k_1, eV/Å^2	k_2, eV/Å^3	k_3, eV/Å^4
Lysozyme	3552	30	−60	60
Water	1600	10	−20	20

are modified with respect to the ones used in Ref. 30 to ensure faster equilibration between the translational and breathing modes for both water and lysozyme molecules. In particular, with the new parameters, the equilibration time is ~6 ps for water at 400 K.

For intermolecular interaction described by the Morse potential, parameters of water-water interaction were chosen to ensure semi-quantitative description of the experimental properties of water. The parameters of non-bonding interactions between lysozyme beads were chosen to roughly reproduce the typical strength of non-bonding interactions in proteins and the equilibrium dimensions of a lysozyme globule.[34] The intramolecular "springs" in the bead-and-spring model, corresponding to the chemical bonds between the polymer units, are described with parameters chosen to represent a typical carbon-carbon bond in polymer molecules.[19]

An intrinsic limitation of any coarse-grained models is the underestimation of the heat capacity of the system due to the reduced number of the dynamic degrees of freedom. For example, a BS "water" particle represents a cluster of 3 water molecules but has only four dynamic degrees of freedom corresponding to the radial breathing and translational motions. This drastically reduces the heat capacity as compared to the real molecular systems. To reproduce the experimental heat capacity of the modeled material, a "heat bath" variable accounting for the energy content of the vibrational modes that are not explicitly represented in the coarse-grained model was introduced.[30,35] Technically, a heat bath temperature is associated with each BS particle, with a heat capacity C^{HB} obtained by subtracting the contributions of the dynamic degrees of freedom from the experimental specific heat of the group of atoms represented by the BS particle, C^{EXP}, i.e., $C^{HB} = C^{EXP} - C^{TR} - C^{R}$, where $C^{TR} = 3k_B$ is the contribution to the heat capacity from the three translational degrees of freedom of the dynamic unit and $C^{R} = k_B$ is the contribution from the radial breathing motion of the unit (k_B is the Boltzmann constant). The heat capacity of water is 4.2×10^3 J/(kg K),[36] which translates to a heat capacity C^{EXP} of 2.18×10^{-3} eV/K per breathing sphere unit with a mass of 50 Da. The heat capacity of anhydrous lysozyme at 25 °C has been determined to be 1.2×10^3 J/(kg K),[37] which translates to a heat capacity C^{EXP} of 1.38×10^{-3} eV/K per polymer bead unit with a mass of 111 Da.

For a BS particle i, the heat bath is directly coupled with its breathing motion by allowing energy exchange between the heat bath and the breathing mode at each time step of the MD integration,

$$C^R \frac{dT_i^R}{dt} = A(T_i^{HB} - T_i^R), \tag{2}$$

$$C^{HB} \frac{dT_i^{HB}}{dt} = -A(T_i^{HB} - T_i^R), \tag{3}$$

where A is a constant that controls the rate of the energy exchange. This constant can be related to the characteristic time τ of the energy exchange between the heat bath and the breathing mode, defined as a time constant of the exponential decay of the difference between the heat bath temperature T_i^{HB} and the breathing temperature T_i^R, as[30]

$$A = \frac{C^{HB}(C^{TR} + C^R)}{(C^{HB} + C^{TR} + C^R)} \frac{1}{\tau}. \tag{4}$$

Note that the coupling between the heat bath and the breathing mode is achieved at the level of individual BS particles. Namely, the heat bath temperature and the breathing temperature in the above equations are defined for each BS particle, i.e., T_i^{HB} and T_i^R for BS particle i. The energy exchange (or coupling) leads to the direct update of the heat bath temperature T_i^{HB}, while for the breathing mode, the energy exchange is achieved dynamically, through an extra "friction" force, $\xi_i M_I v_i^R$, added to the equations of motion solved for the breathing/radial degrees of freedom of the BSs,

$$M_I \frac{d^2 R_i}{d^2 t} = F_i^R + \xi_i M_I v_i^R, \tag{5}$$

where v_i^R is the instantaneous velocity of radial motion of particle i, F_i^R is the force acting on the radial degree of freedom of particle i due to the interaction with other particles, and coefficient $\xi_i = A \times (T_i^{HB} - T_i^R)/k_B T_i^R$ ensures the desired energy transfer and energy conservation.

The laser excitation is simulated by depositing quanta of energy equal to the photon energy into the heat bath of the absorbing BS water molecules randomly chosen during the laser pulse duration. The total number of photons entering the model during the laser pulse is determined by the laser fluence, and the probability of a molecule to be excited is modulated by the Lambert–Beer's law to reproduce the exponential attenuation of the laser light with depth. The laser penetration depth of 2 μm is used in the simulations.[7] The laser energy deposited to the heat bath is transferred to the breathing motion through the coupling between the heat bath and the breathing mode and then finally transferred to the translational motion through the dynamic coupling between the breathing and translational modes as discussed above. The value of τ in Eq. (4) was selected to be 1 ps in order to achieve the same time scale for vibrational relaxation as reported in a recent spectroscopy study of liquid water.[38]

The interaction of the BS particles in the solution with the rigid optically transparent substrate (representing the conducting plate in Fig. 1) is assumed to be 3 times stronger than the interactions between BS water particles. The dimensions of the computational cell in the directions parallel to the surface are fixed at 20×20 nm^2, and the periodic boundary conditions are applied in these directions. The whole computational cell consists of 338 755 BS water particles, corresponding to 935 983 real water molecules, and 140 lysozyme chains, corresponding to a lysozyme concentration of 8.3 mM, similar to that found in cellular environment.[27]

To prepare the ionic lysozyme solution, for simplicity, instead of the explicit introduction of positive salt ions and counter-ions (Fig. 1), a single positive charge (1 e^+) is assigned to a randomly selected polymer bead of each polymer chain representing a lysozyme molecule. In order to have net zero charge in the system, a negative charge was then assigned to a neighboring BS water particle for each positively charged polymer bead, at the initial distance close to 5.4 Å, the minimum distance between salt ions and counter-ions in salt saturated solution reported in the literature.[39] Conventionally, the Ewald summation technique is applied for the treatment of long-range electrostatic interactions.[40] Here, however, we employed a simple alternative utilizing the extended boundary conditions to calculate interionic interactions,[41] where each individual charged particle interacts not only with the other charged particles in the original volume, but also with charges in 24 replicated volumes surrounding it in the lateral directions. The initial system used in all PIRL-DIVE simulations was equilibrated at 300 K. In addition to the plume dynamics, the simulations were also used to study the protein-counter-ion separation under different electric field conditions.

III. RESULTS OF MD SIMULATIONS AND DISCUSSION

In this section, the general properties of PIRL-DIVE ablation plume with and without electric field are first reviewed, followed by a detailed analysis of the characteristics of ions and molecules in the ablation plume, and the discussion of the effect of the electric field and its implication on the desorption and ion separation.

A. Parameters of PIRL-DIVE ablation plume in external electric field

The system evolution following PIRL-DIVE ablation in the absence of electric field is shown in Fig. 2 in terms of the kinetic energies in the heat bath, breathing mode, and translational mode. The energies are expressed in temperature units by normalization with the corresponding heat capacities for easier comparison. The laser energy (black line in Fig. 2) is modeled to be directly deposited into the heat bath (blue line in Fig. 2) and is then redistributed and transferred into the translational motion driving the PIRL-DIVE ablation almost instantaneously through the above discussed coupling algorithm. The energy deposition and redistribution in the simulation mimics the PIRL-DIVE process where the laser energy deposited into the OH vibration stretch mode quickly transfers, through the water hydrogen bond network, into the translational motion. For the breathing mode and the heat bath, the normalized kinetic energy can be considered as the temperature, and they converge with each other due to their direct coupling. The fast energy transfer to the translational motion drives the ablation and collective expansion of the ablation plume, leading to the continuous increase of the normalized kinetic energy of the translational motion.

The evolution of plume's total energy W_{total} under the four electric field conditions is shown in Fig. 3. For the extreme field of E = 10^{10} V/m (blue), W_{total} begins to exceed the W_{total} without electric fields (red) at 500 ps. This significant increase in the total energy of the ablation plume comes from the energy that the ions gain from the electric field, and it is undesirable in the experiment since it can lead to severe fragmentation as will be confirmed later. Under typical TOF-MS conditions, E = 10^7 V/m (green) and E = -10^7 V/m (purple), W_{total} follows nearly the same evolution as under the condition, E = 0 V/m (red), with a rapid increase between 200 and 300 ps when the peak of PIRL pulse arrives, reaching a plateau shortly after 300 ps. The similar evolution of the system's total energy under a typical TOF-MS condition implies that such an electric field does not significantly heat the PIRL-DIVE plume within the first 1 ns of ablation compared to the case of no electric field applied. This means that it is quite likely that the lysozyme ions will remain intact for analysis as if they were desorbed by PIRL-DIVE ablation without an applied electric field.

The system evolution is further illustrated with the contour plot of the temperature associated with the thermal

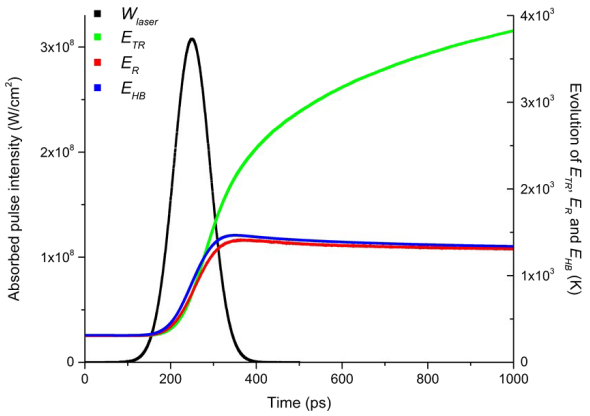

FIG. 2. Laser energy deposition and evolution of different components of the kinetic energy in ablation without electric field (E = 0 V/m). Black curve: absorbed pulse intensity (W_{laser}); green curve: kinetic energy associated with system's translational motion (E_{TR}); red curve: kinetic energy associated with system's breathing motion (E_R); blue curve: kinetic energy associated with system's heat bath (E_{HB}).

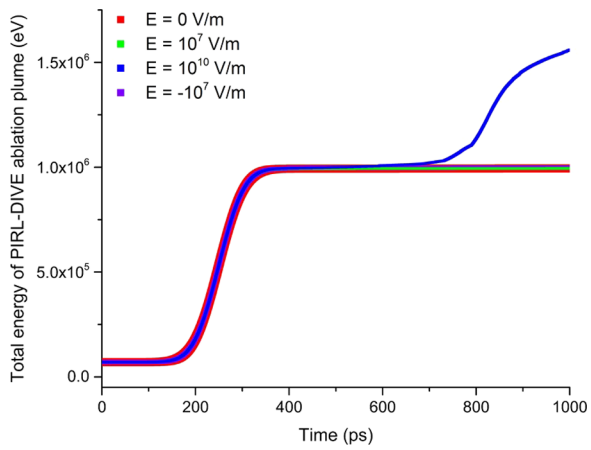

FIG. 3. The evolution of the total energy of PIRL-DIVE ablation plume predicted in simulations performed with four different values of the electric field.

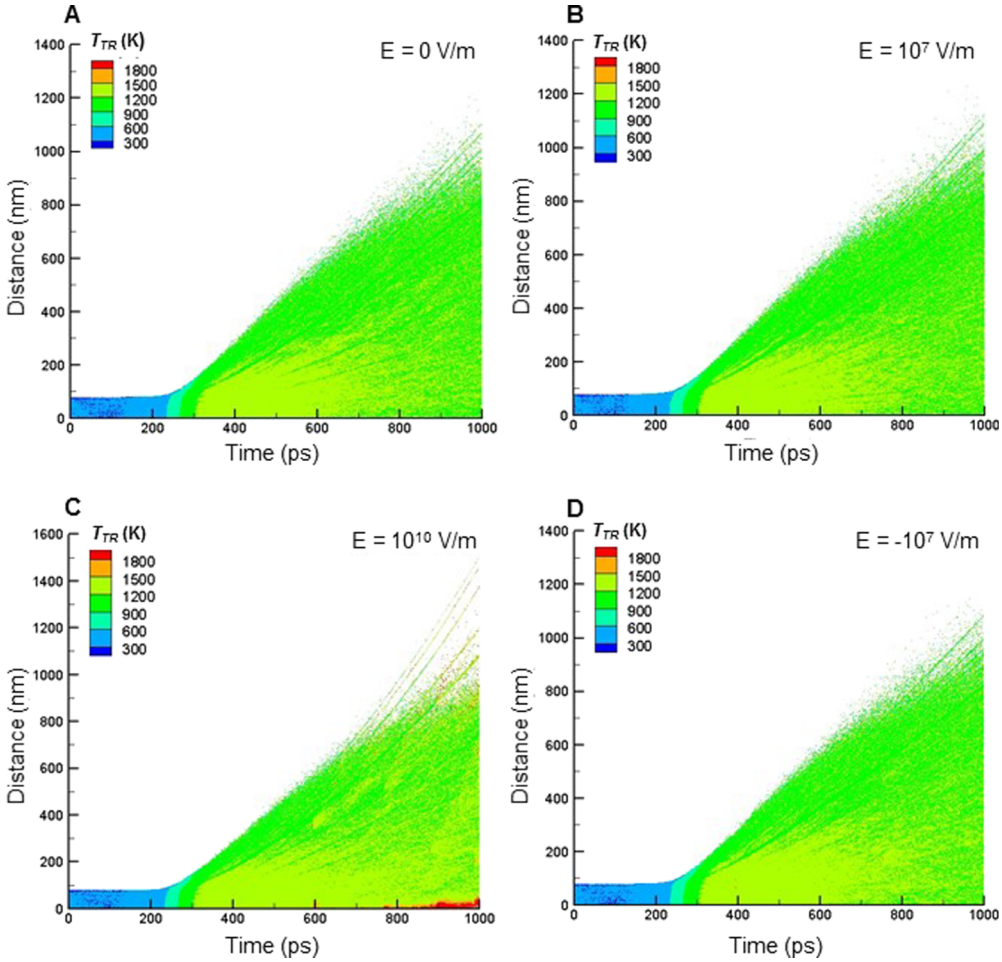

FIG. 4. Contour plot showing spatial-temporal evolution of the translational temperature of ablation plume expanding under four electric field conditions: (a) no electric field applied; (b) 10^7 V/m applied along plume propagation direction; (c) 10^{10} V/m applied along plume propagation direction; (d) -10^7 V/m applied opposite to the plume propagation direction.

translational motion T_{TR}, shown in Fig. 4. In contrast to E_{TR} plotted in Fig. 2, the temperature T_{TR} is calculated from thermal velocities of molecular motions obtained by subtracting the contributions from the center-of-mass velocities of the local regions the molecules belong to. Under the extreme electric field condition, E = 10^{10} V/m (Fig. 4(c)), regions with increased temperature (red), T_{TR} > 1800 K, begin to appear in the vicinity of the substrate at 500 ps post-ablation. This zone grows up to 50 nm above the substrate at 1 ns post-ablation. Numerous hot spots (red dots) with T_{TR} > 1800 K in the upper portion of the plume also appear after 500 ps of ablation. These hot areas and spots are due to the collision of ions with the rigid substrate and the surrounding molecules and are undesirable though expected for the extreme field conditions. For typical TOF-MS electric field conditions, E = 10^7 V/m (Fig. 4(b)) and E = -10^7 V/m (Fig. 4(d)), there is no observable difference in T_{TR} as compared to E = 0 V/m (Fig. 4(a)). The front layer of the plume propagates 1300 nm within 1 ns, corresponding to a plume velocity of 1300 m/s, similar to the results (1500 m/s) obtained by continuum-level Euler hydrodynamics numerical simulation of pure liquid water under a slightly lower fluence (0.7 J/cm^2).[7] The temperature T_{TR} begins to increase at 200 ps, reaches a peak level of around 1300 K by 500 ps, and then gradually decreases due to the plume expansion. The contour plot further illustrates that the extremely large electric field significantly increases the plume temperature, which is undesirable in experiment. However, the electric field used in typical TOF-MS experiments (E = ±10^7 V/m) minimally affects the PIRL-DIVE ablation process, which will simplify the design of the actual ion source.

B. Characteristics of ions and molecules in the ablation plume

The molecules and ions contained within the ablation plume generated in PIRL-DIVE ablation were individually examined and their characteristics were compared under various external field conditions. The number of water molecules interacting with each bead composing the lysozyme chain, N_w, was examined to characterize the desolvation process following ablation. As described in Section II, each lysozyme chain was composed of 129 beads with a total of 140 lysozyme chains in the system, resulting in 18 060 beads in total. Fig. 5 shows the average number of BS water molecules interacting with each bead, N_w, averaged over the 18 060 beads for each of the four simulated electric field conditions. As expected, the desolvation process is synchronized with the

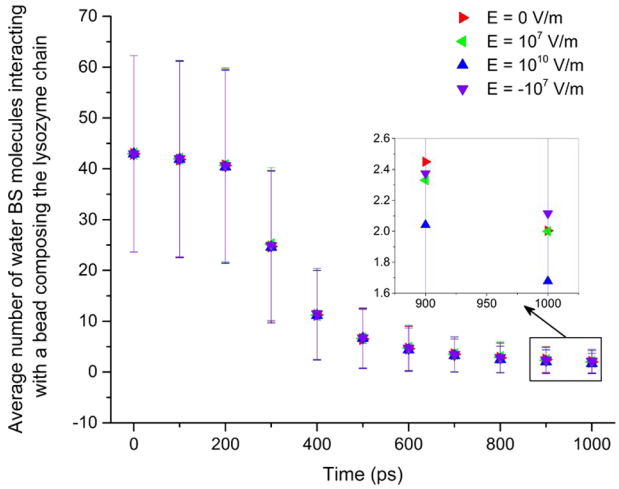

FIG. 5. Average number of water BS molecules interacting with a bead composing a lysozyme chain. The inset is a zoom-in view of the last two data points. The error bars indicate the standard deviation of the mean of the data set.

laser ablation, indicated by the rapid drop of N_w at 200–300 ps as shown in Fig. 5. This corresponds to the significant increase of the system's total energy, shown in Fig. 3, indicating that the ablation process is the direct consequence of the laser energy absorption by water molecules. Furthermore, for all the four simulated scenarios, the desolvation process is quite similar, as can be seen from the overlay of the data points in Fig. 5 and the inset showing a zoom-in view of the last two data points. For all simulated scenarios, each lysozyme bead initially interacts with ~42 BS water molecules on average. This number rapidly decreases down to ~2 for each bead by the time of 1 ns. Though complete desolvation was not achieved, the reduction of number of water molecules interacting with each lysozyme bead by more than 90% within just 1 ns indicates an extremely efficient desolvation process following PIRL-DIVE ablation. More importantly, the desolvation process is entirely due to the ablation process driven by the energy absorption by water molecules and thus is independent of the applied external electric field, as indicated by the similar evolution of N_w in the four simulations shown in Fig. 5. This characteristic of the desolvation process in PIRL-DIVE ablation could be beneficial for the design of a quantitative ion source, as it reflects the decoupling of the ionization from desolvation, which will allow optimization of the two processes independently.

Peptide fragmentation during ablation was also investigated. Ideally, the mass spectrum acquired from a quantitative ion source should only be composed of molecular ions from the original biological sample. In principle, there should be minimal fragmentation of lysozyme from PIRL-DIVE ablation, as the deposited laser pulse energy is transferred to the translational motion of water to drive the ablation, and the energy transfer process occurs on a time scale that is faster than any other energy transfer mechanism.[8] For the simulated scenarios presented here, the lysozyme is charged and counter-ions exist for charge balance. The energy and temperature evolution of the plume, Figs. 3 and 4, indicate that the electric field under typical TOF-MS conditions contributes minimally to the system's total energy and the dynamics of the plume and thus little fragmentation is expected. In order to characterize the fragmentation process, the number of fragmented lysozyme molecules, N_f, is counted. The initial system contains 140 lysozyme chains each of which is composed of 129 monomer beads. At each time step, the number of intact lysozyme chains that were still composed of 129 beads was counted. This number was then subtracted from the initial 140 intact lysozyme chains, resulting in N_f, the number of fragmented lysozyme molecules. The evolution of N_f is shown in Fig. 6. It is illustrated in Fig. 6 that the extreme electric field condition, $E = 10^{10}$ V/m (blue up triangles), leads to enhanced fragmentation, with 33 lysozymes fragmented by the time of 1 ns post-ablation, which corresponds to ~24% fragmentation. Under a typical TOF-MS condition, positive field $E = 10^7$ V/m (green left triangles), the fragmentation process is found to be similar to the one under condition of no applied electric field (red right triangles), with only ~2% fragmentation corresponding to 3 fragmented lysozymes observed by 1 ns. When a negative electric field is applied, the fragmentation is enhanced slightly (purple down triangles) which is likely to be related to the fact that the fast low mass negative ions are further accelerated by the electrical field, leading to a higher probability of energetic collisions with surrounding molecules. A total of 8 lysozyme chains were fragmented in this case by 1 ns post-ablation, which corresponds to ~6% fragmentation. Thus under typical TOF-MS conditions with a positive electric field applied, the fragmentation process is not significantly enhanced. Furthermore, the PIRL-DIVE ablation is very soft to large molecules such as lysozyme, with only 2% of lysozyme molecules fragmented at a laser fluence above the ablation threshold, compared to 7% fragmentation in UV-MALDI experiments performed for organic solid thin films irradiated at laser fluences below the ablation threshold.[42,43]

The results all imply that, under typical TOF-MS conditions, the electric field has no significant effect on the PIRL-DIVE ablation plume dynamics as well for the desolvation and fragmentation of individual lysozyme molecules. In the simulations, each lysozyme molecule is

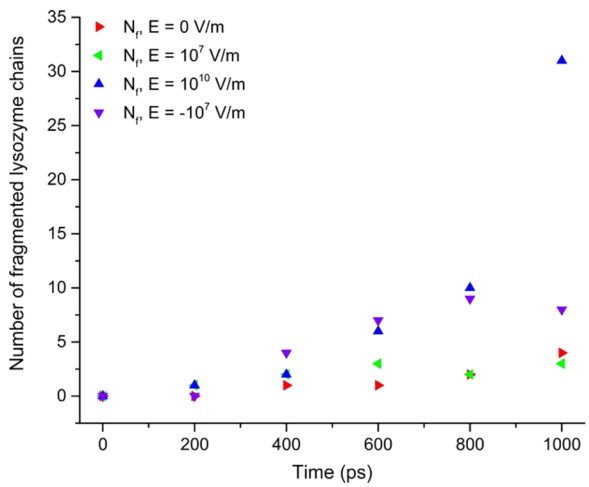

FIG. 6. Number of lysozyme molecules fragmented during PIRL-DIVE ablation (out of the total of 140).

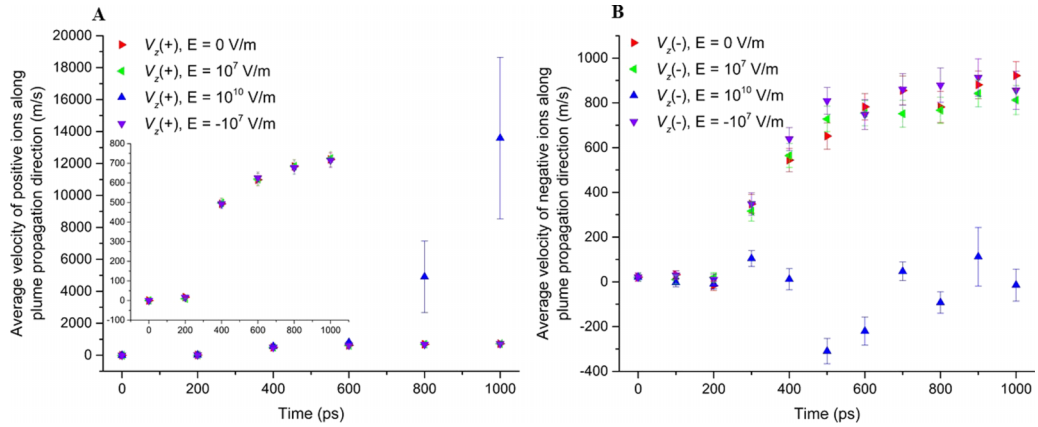

FIG. 7. Average velocity along plume propagation direction V_z of (a) positive ions and (b) negative ions. The inset in (a) shows an enlarged view of the same data, with the results for E = 10^{10} V/m excluded.

singly charged to mimic an analyte in actual experiments, allowing us to also investigate how the electric field affects the individual ion motion. The evolution of the average velocity of positive ions (lysozyme) $V_z(+)$ and negative ions (water) $V_z(-)$ along the plume propagation direction was calculated within 1 ns of ablation under the four simulated electric field conditions, and the results are shown in Fig. 7. Under the extreme field condition (E = 10^{10} V/m), the electric field significantly increases the velocity of positive ions (blue up triangles, Fig. 7(a)) whereas under typical TOF-MS conditions (Fig. 7(a) inset), E = 10^7 V/m (green left triangles) and E = -10^7 V/m (purple down triangles), the average velocity of positive ions remains similar to the case of PIRL-DIVE with E = 0 V/m (red right triangles), reaching 700 m/s by 1 ns post-ablation. The average velocity of the negative counter-ions along the plume propagation direction is shown in Fig. 7(b). Here again, under the extreme condition of E = 10^{10} V/m, the electric field drives the negative ions to propagate towards the substrate (IR transparent conductive plate in Fig. 1), opposite to the plume expansion direction, resulting in negative values of the average velocity at 400 ps post-ablation, Fig. 7(b) (blue up triangles). However, under the typical MS condition, E = 10^7 V/m (green left triangles, Fig. 7(b)) and E = -10^7 V/m (purple down triangles, Fig. 7(b)), the negative ions propagate at velocities similar to those in PIRL-DIVE with E = 0 V/m (red right triangles, Fig. 7(b)), that is, ~800 m/s at 1 ns post-ablation, higher than the velocity of positive ions (~700 m/s) due to the lighter mass of counter-ion molecules. The average velocities of positive ions (Fig. 7(a)) and negative ions (Fig. 7(b)) both indicate that, under the typical TOF-MS condition, E = $\pm 10^7$ V/m, the motion of ions within the first 1 ns post-ablation is defined by the ablation dynamics, with the electric field having a negligible effect.

The average position of positive (lyzoyme) $d_z(+)$ and negative (water) $d_z(-)$ ions along the plume propagation direction was also analyzed and the results are shown in Figs. 8(a) and 8(b), respectively. Positive ions propagated faster under the extreme condition of E = 10^{10} V/m and thus move further away from the substrate ($d_z = 0$) as shown by the blue up triangles in Fig. 8(a), whereas negative ions were driven into the substrate as indicated by the blue up triangles in Fig. 8(b). These negative ions collide with the rigid substrate as well as with surrounding molecules, leading to the appearance of the layers of increased temperature in the vicinity of substrate shown in Fig. 4(c) in Section I. For comparison, the average positions of positive ions under the typical TOF-MS conditions of E = 10^7 V/m (green left triangles in the inset in Fig. 8(a)) and E = -10^7 V/m (purple

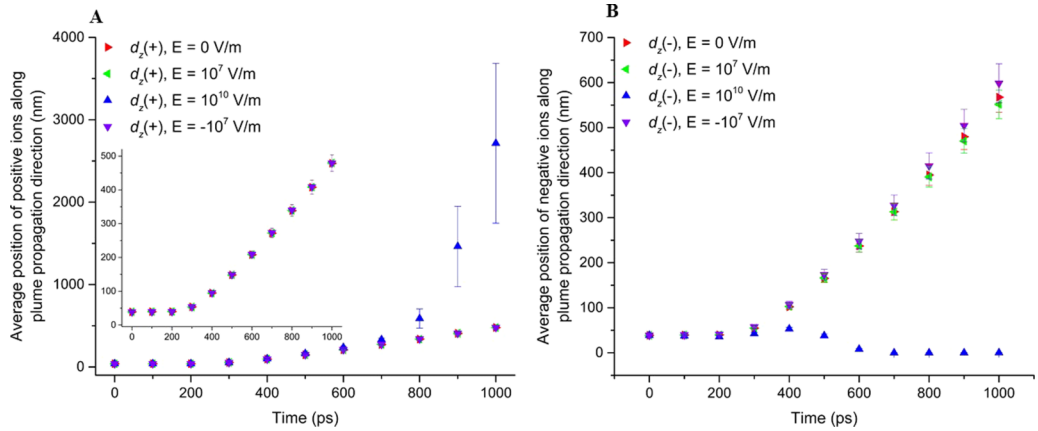

FIG. 8. Average position along plume propagation direction d_z of (a) positive ions and (b) negative ions. The inset in (a) shows an enlarged view of the same data, with the results for E = 10^{10} V/m excluded.

down triangles in the inset in Fig. 8(a)) were nearly identical to those observed in the case with no applied electric field (red right triangles in the inset in Fig. 8(a)). The first appearance of the effect of the electric field on ion separation under typical TOF-MS conditions of E = 10^7 V/m and E = -10^7 V/m can be seen in Fig. 8(b). At times t > 700 ps, the negative ions are located on average slightly closer to the substrate when a field of E = 10^7 V/m (green left triangles, Fig. 8(b)) is applied and further away from the substrate when the direction of the field is reverse, E = -10^7 V/m (purple down triangles, Fig. 8(b)), as compared to the case with no applied electric field (red right triangles, Fig. 8(b)).

In order to further investigate the effect of the electric field on the ion separation process, the average distance between positive and negative ions along the plume propagation direction D_z was calculated as $D_z = d_z(+) - d_z(-)$ and is shown in Fig. 9. Under the extreme electric field of E = 10^{10} V/m, the positive and negative ions are rapidly separated (blue up triangles, Fig. 9), to approximately 2500 nm by 1 ns post-ablation, with positive ions propagating further away and negative ions pushed closer to the substrate by the electric field (Fig. 8). The PIRL-DIVE ablation itself also results in ion separation (red right triangles, Fig. 9 inset), due to the faster propagation of lighter negative counter-ions (water) as compared to the more massive positive ions (lysozyme), resulting in a gradually increasing negative value of D_z. The average distance between positive and negative ions in the field-free simulation increased to ~80 nm by 1 ns post-ablation (red right triangles, Fig. 9 inset). Under typical TOF-MS conditions, the electric field enhances (E = -10^7 V/m, purple down triangles, Fig. 9 inset) or suppresses (E = 10^7 V/m, green left triangles, Fig. 9 inset) the ion separation process at this initial stage of the ablation plume expansion. This is due to the enhanced initial velocity of the counter-ions as compared to the peptide in combination with the effect of the electric field imparting an increased/decreased velocity to the counter-ions depending on the direction of the applied field to either enhance or suppress ion separation within the plume. At a later stage of ablation (t > 1 ns), the ion separation can be enhanced by the positive electric field once the negative ions are turned back to propagate towards the substrate, as suggested by the results obtained for the extreme electric field. The slow and soft ion separation process is advantageous for designing a quantitative ion source. Further, it is possible that the insights into the effect of the electric field on the charge separation in the plume, revealed in the simulations, may be utilized in designing a more efficient, multi-pulse, bi-directional field ion separation, extraction, and TOF analysis protocol.

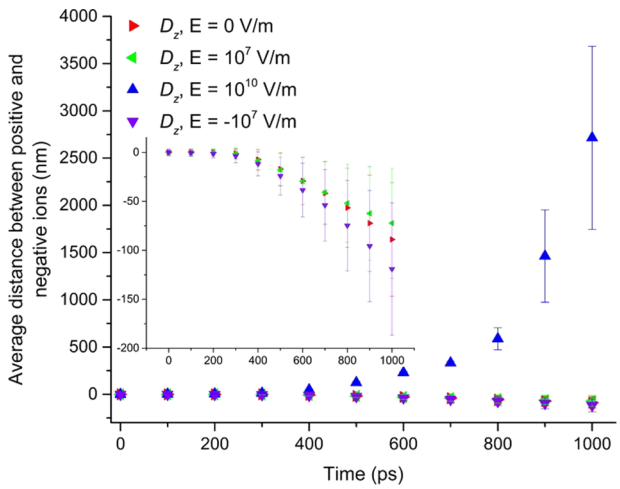

FIG. 9. Average distance D_z between positive and negative ions along the plume propagation direction. The inset shows an enlarged view of the same data, with the results for E = 10^{10} V/m excluded.

C. Discussion

The MD simulations of laser ablation of aqueous solutions of lysozyme ions suggest that the PIRL-DIVE mechanism is very promising with respect to the development of quantitative ion source capable of direct MS analysis of complex biological samples. The desorption of lysozyme was shown to be efficient with significant and rapid reduction in the average number of water molecules interacting with polymer molecules within the first nanosecond of the ablation plume expansion. The desolvation process is initiated by the PIRL pulse energy deposition into the system and is found to be largely unaffected by the applied electric field, as indicated by Fig. 5. Under extreme field conditions, the total energy of the system is significantly increased (Fig. 3) and areas of high temperature with T_{TR} > 1800 K appear in the plume (Fig. 4(c)) due to the collisions of significantly accelerated positive lysozyme ions with surrounding molecules as well as the collisions of negative ions driven by the electric field with the substrate. The simulations further show that under the typical TOF-MS conditions (E = ±10^7 V/m), the electric field does not significantly contribute to heating of the plume (Fig. 3) and thus does not affect the plume dynamics, with the results comparable to the standard PIRL-DIVE (E = 0 V/m). The electric field under typical TOF-MS conditions does not induce significant fragmentation (Fig. 6), indicating that molecules ablated inside the TOF-MS should have similar characteristics to molecules produces by ablation in the absence of the electric field, which are intact and undamaged.

However, some fragmentation was observed in the simulations even in the absence of electric field. The laser fluence used here was the same as experimentally utilized for MS imaging of tissue samples,[17] which is probably too high for the ablation of a thin film of water. The fragmentation process can be controlled by adjusting the incident laser fluence.[30] MD simulations utilizing a lower PIRL fluence will be considered to minimize the fragmentation and optimize the desolvation process. Even so, the degree of fragmentation at such a high fluence, with an excitation level well above the ablation threshold, was significantly lower than that characteristic of conventional MALDI experiments, and even lower than the degree of fragmentation observed in laser desorption experiments performed below the ablation threshold.[42,43]

Under typical TOF-MS conditions, the electric field affects the ions' motion in a slow and soft manner with the ablation dominating the ions' motion in the first 1 ns and the electric field only contributing at later times. For positively charged lysozyme, this is reasonable due to its large

molecular mass. During the first nanosecond of the ablation plume expansion, lysozyme ions propagate to approximately 500 nm (Fig. 8(a) inset, green) from the substrate and reach an average velocity of 700 m/s (Fig. 7(a) inset, green left triangles). Assuming the propagation occurs in vacuum for a free lysozyme in an electric field of 10^7 V/m, an ion would obtain 5 eV of kinetic energy from the electric field over this distance (500 nm). This translates to a velocity increase of the lysozyme ion from 700 m/s to 746 m/s. For ions propagating within the ablation plume, charge screening and collisions with other molecules would further reduce the effect of the electric field. Thus the electric field effect on the lysozyme ions can be considered negligible at this stage of ablation. For a negatively charged counter-ion molecule with mass of 50 Da and velocity of 800 m/s (Fig. 7(b) inset, green left triangles), over 500 nm (Fig. 8(b) inset, green left triangles) of propagation in vacuum, the electric field accelerates the ions in the opposite direction up to a speed of ~4300 m/s. For the field applied opposite to the plume propagation direction, the velocity of negative ions can be increased from 800 m/s to ~4500 m/s, which is a very large effect. However, the scenario is different if negative ions propagate within a plume with a molecular number density which is 1.3×10^{-2} Å^{-3} initially and then reduces to 7.5×10^{-4} Å^{-3} by 1 ns of the plume expansion, as they are in the present simulation. The ions' motion is not only governed by the electric field, but also strongly affected by the interaction with the surrounding molecules. Assuming the moving plume as the reference frame, each molecular collision randomly effects the direction of the velocity of negative ions. The electric field, however, will bias the ion motion between the collisions, leading to the appearance of a drift velocity of negative ions. The effect is similar to the motion of electrons in a conductor with an applied electric field if we consider the plume as the reference frame. Thus, the drift velocity of ions in the reference frame of the plume can be determined in a manner similar to that used in the analysis of the drift of electrons in a conductor in the presence of an electric field.

In the plume, an ion with charge q experiences an electric force of $F_e = qE$. The drift velocity v_d is given by $v_d = \tau_f(qE/m)$, assuming that the velocity after each collision is random in the plume reference frame, and τ_f is the mean free time between successive collisions. For simple estimation, the plume is treated as a gas, the mean free path is evaluated as $D = 1/(\sqrt{2}\sigma n)$, where σ is collisional cross section and n is the gas (plume) density. The characteristic interaction distance between particles in our system is $d \sim 4.6$ Å which is approximated as the nearest distance between particles in a face-centered cubic crystal structure with BS water density. This gives an estimation of the collision cross section being $\sigma = \pi d^2 = 66.5$ Å^2. The density of the plume at 1 ns is $n = 7.5 \times 10^{-4}$ Å^{-3}. Thus the mean free path is estimated to be $D = 14.1$ Å. The temperature of the plume at 1 ns of ablation is ~1000 K (Fig. 4), which gives the mean velocity of $v = \sqrt{(3k_BT/m)} = 7$ Å / ps = 700 m/s, where k_B is the Boltzmann constant and m is the mass of a water BS particle (50 Da). Thus, the mean free time between collisions, $\tau_f = D/v \sim 2$ ps, leads to a drift velocity of $v_d = \tau_f(qE/m) \sim 40$ m/s, which is ~5% of the total plume velocity of 700 m/s. This explains why under TOF-MS conditions the electric field (E = $\pm 10^7$ V/m) modifies the ions' motion in such a gentle way. As the plume expands further, the density of the plume becomes lower, resulting in a longer mean free time for collisions. The electric field should then play an increasingly important role in the ions' motion, contributing to the charge separation and improving the ion signal in the MS spectra.

To verify the above deduction, the simulations performed under conditions of pure PIRL-DIVE ablation (E = 0 V/m) and typical TOF-MS (E = 10^7 V/m) were continued until 2 ns post-ablation. The velocity of ions along the plume propagation direction is shown in Fig. 10. The first sign of the electric field effect on positive ion motion is observed in Fig. 10(a) at 1.8 ns, when the velocity of positive ions under the TOF-MS condition (green left triangles, Fig. 10(a)) becomes higher than the case of PIRL-DIVE with no applied field (red right triangles, Fig. 10(a)). The velocities of negative ions, plotted in Fig. 10(b), show a significant difference between the typical TOF-MS conditions (green left triangles) and PIRL-DIVE with no applied field (red right triangles) starting from ~1.6 ns post-ablation. At a time of 2 ns, average velocity of negative ions generated under typical TOF-MS conditions (green left triangles) is ~300 m/s lower than the one in the case with no applied field (red). This indicates that,

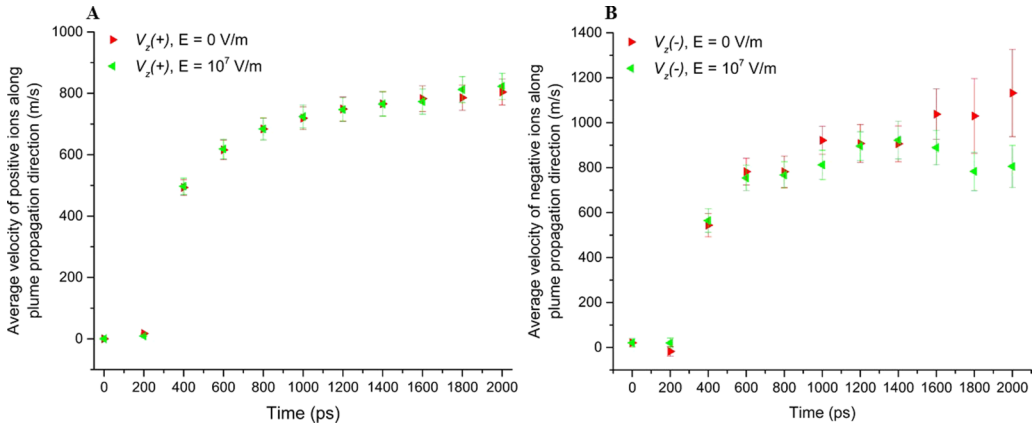

FIG. 10. Average velocity of ions along the plume propagation direction, V_z, calculated up to 2 ns of the ablation plume expansion: (a) velocity of positive ions; (b) velocity of negative ions.

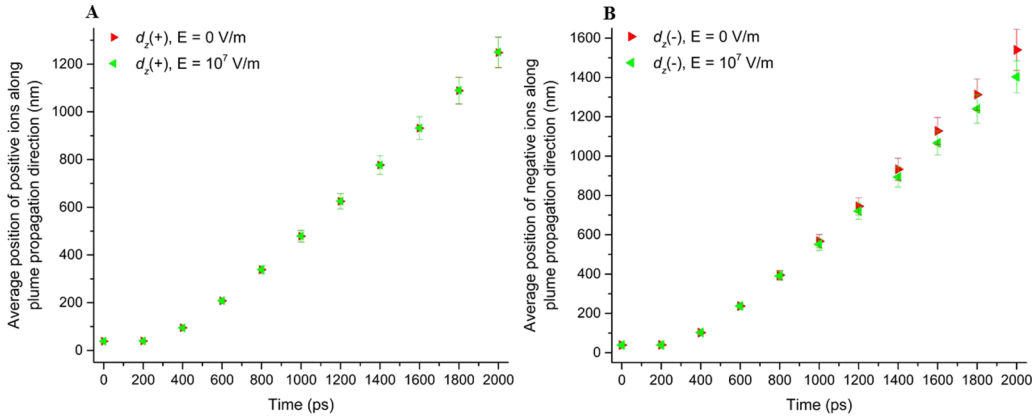

FIG. 11. Average position of ions along the plume propagation direction, d_z, calculated up to 2 ns post-ablation: (a) position of positive ions; (b) position of negative ions; green, electric field of E = 10^7 V/m applied; red, no electric field applied E = 0 V/m.

at this stage of the ablation process, the density of the plume is sufficiently low for the electric field to significantly affect the ion's motion.

The average position of positive ions $d_z(+)$ and negative ions $d_z(-)$ along the plume propagation direction is shown in Figs. 11(a) and 11(b), respectively, until 2 ns post-ablation. The position of positive ions follows the same trend under typical TOF-MS conditions (green left triangles, Fig. 11(a)) as in PIRL-DIVE with no applied field (red right triangles, Fig. 11(a)). The field-induced slowdown of the negative ions under typical TOF-MS conditions leads to the position of the negative ions shifted closer to the substrate (green left triangles, Fig. 11(b)) as compared with the ones in PIRL-DIVE simulation with no applied field (red right triangles, Fig. 11(b)). Thus, the average distance between the positive and negative ions, $D_z = d_z(+) - d_z(-)$, is smaller under typical TOF-MS conditions (green left triangles, Fig. 12) than in PIRL-DIVE with no applied field (red right triangles, Fig. 12). As the ablation proceeds to 2 ns post-ablation, Figs. 10–12, the ion separation process continues and the electric field influence on the ions' motion becomes more significant.

The results indicate that the separation of positively charged analyte ions from their associated counter-anions can be enhanced by the electric field at later times. The mass spectra produced from this type of direct desolvation and counter-ion removal would directly reflect the intrinsic charge state of the molecule in aqueous solution, more similar in form to those produced by ESI type measurements or native MS for analytes directly extracted from biological conditions. The charge distribution could be further modified by changing the pH of the solution, increasing the population of protonated or negatively charged sites. This mechanism of desolvation and ion formation could be applied to analytes in real biological systems containing additional negatively charged species, such as lipids, as the mechanism is equivalent for the removal of their typically associated, low mass salt counter-cations. For systems containing electrostatically associated negatively and positively charged analytes of similar masses, the ion separation process can be expected to be slower due to the reduced drift velocity. Given the nature of the ablation process, which couples directly to the solvent water molecules on an ultrafast time scale, the desolvation and stripping off of counter-ions from the charged species is not dependent on the presence of contaminants which can compete for the charge causing ion suppression effects as is common in nebulization based ionization methods. Thus a PIRL-DIVE based ion source has significant potential as an intrinsically ion suppression free source capable of quantitative analysis of complicated biological system.

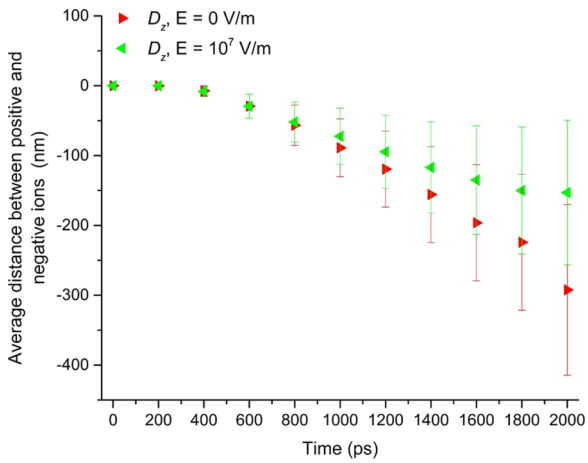

FIG. 12. Average distance between the positive and negative ions along the plume propagation direction, D_z, shown up to 2 ns of the ablation plume expansion.

IV. CONCLUSION AND PERSPECTIVE

In the present study, MD simulations of the PIRL-DIVE ablation process were performed on a charged peptide/counter-ion system in aqueous solution. Computational predictions obtained for achievable TOF-MS conditions (E = ±10^7 V/m) for ion extraction are compared with both the standard PIRL-DIVE process (E = 0 V/m) and the one under extreme field conditions (E = 10^{10} V/m). The results indicate that under typical TOF-MS conditions, the electric field does not impart a significant amount of energy to the system and the initial plume dynamics is retained. Efficient desorption and desolvation of lysozyme is observed and the process is synchronized with the laser energy deposition and is totally independent of the applied electric field. This characteristic of

the PIRL-DIVE ablation process has important implications for the development of a quantitative ion source. In both ESI and MALDI, it is not possible to independently optimize the desorption and ionization process. However, in the PIRL-DIVE ablation process, as predicted in the present work, the desorption and ionization processes can be optimized independently, by first optimizing the desorption process by adjusting the PIRL pulse fluence and then adjusting the ion separation process by applying the proper electric field. Given that water, making up more than 90% of biological materials, is the medium for PIRL-DIVE coupling, the optimization of the desorption process is independent of the presence of analytes in the aqueous solution as well as the process of stripping counter-ions off from charged sites located on the analyte molecules. The charge state and mass of the analyte ions will affect the rate of field-induced ion/counter-ion separation, though complete separation could be achieved given adequate time. Thus, the optimization of ion separation is independent of solution contaminants as well as analyte molecule properties, such as their mass, polarity, and chemical activity. These unique properties endow an ion source based on the PIRL-DIVE ablation as intrinsically versatile and sensitive. The high sensitivity and versatility of PIRL-DIVE as an ion source are crucial for the analysis of complicated biological samples, which can contain thousands of different molecules with their concentrations ranging from pico-molar to milli-molar. Though slight fragmentation was observed even under standard PIRL-DIVE conditions, the electric field present in typical TOF-MS conditions did not enhance fragmentation, indicating the viability of the method for extracting intact and undamaged biological molecules.

The electric field inside a typical TOF-MS ($E = 10^7$ V/m) is found to enhance the ion separation in a soft manner, unlike under the extreme field condition of $E = 10^{10}$ V/m, where the ion separation is completed within the first nanosecond after the ablation onset and a severe molecular fragmentation is observed. For standard TOF-MS fields, as ablation proceeds, the motion of the ions and complete ion separation are achieved at a later stage of the ablation plume expansion, as predicted by the longer time simulations continued until 2 ns post-ablation. To create a complete picture of the desorption and ion separation, as well as minimize fragmentation, further simulations investigating lower PIRL fluence and weaker electric fields ($<10^7$ V/m) will be performed with simulations extended to longer times. PIRL-DIVE ablation is a promising approach to the development of an ion source that is intrinsically quantitative, sensitive, and versatile, possibly allowing analysis of complex samples with little to no preparation.

ACKNOWLEDGMENTS

The authors wish to thank Compute Canada for help with the code implementation on their cluster SCINET. The financial support of this work was provided by the Max Planck Society and the National Science Foundation (NSF) through Grant No. CMMI-1301298. R. J. Dwayne Miller is the author of a patent related to the mechanism of PIRL laser ablation.

[1]M. Karas, D. Bachmann, and F. Hillenkamp, Anal. Chem. **57**, 2935 (1985).
[2]M. Yamashita and J. B. Fenn, J. Phys. Chem. **88**, 4451 (1984).
[3]M. E. Belov, M. V. Gorshkov, H. R. Udseth, G. A. Anderson, and R. D. Smith, Anal. Chem. **72**, 2271 (2000).
[4]M. Kandiah and P. L. Urban, Chem. Soc. Rev. **42**, 5299–5322 (2013).
[5]S. Jespersen, W. M. A. Niessen, U. R. Tjaden, J. van der Greef, E. Litborn, U. Lindberg, J. Roeraade, and F. Hillenkamp, Rapid Commun. Mass Spectrom. **8**, 581 (1994).
[6]A. Bodzon-Kulakowska, A. Bierczynska-Krzysik, T. Dylag, A. Drabik, P. Suder, M. Noga, J. Jarzebinska, and J. Silberring, J. Chromatogr. B **849**, 1 (2007).
[7]K. Franjic and R. J. D. Miller, Phys. Chem. Chem. Phys. **12**, 5225 (2010).
[8]M. L. Cowan, B. D. Bruner, N. Huse, J. R. Dwyer, B. Chugh, E. T. J. Nibbering, T. Elsaesser, and R. J. D. Miller, Nature **434**, 199 (2005).
[9]P. Nemes and A. Vertes, Anal. Chem. **79**, 8098 (2007).
[10]P. Nemes, A. S. Woods, and V. Vertes, Anal. Chem. **82**, 982 (2010).
[11]S. Amini-Nik, D. Kraemer, M. L. Cowan, K. Gunaratne, P. Nadesan, B. A. Alman, and R. J. D. Miller, PLoS One **5**, e13053 (2010).
[12]K. Franjic, M. L. Cowan, D. Kraemer, and R. J. D. Miller, Opt. Express **17**, 22937 (2009).
[13]N. Jowett, W. Wöllmer, A. M. Mlynarek, P. Wiseman, B. Segal, K. Franjic, P. Krötz, A. Böttcher, R. Knecht, and R. J. D. Miller, JAMA Otolaryngol.–Head Neck Surg. **139**, 828 (2013).
[14]H. Petersen, F. Tavakoli, S. Kruber, A. Münscher, A. Gliese, N. O. Hansen, S. Uschold, D. Eggert, W. D. Robertson, T. Gosau, S. Sehner, M. Kwiatkowski, H. Schlüter, U. Schumacher, R. Knecht, and R. J. D. Miller, Lasers Surg. Med. **48**, 385 (2016).
[15]M. Kwiatkowski, M. Wurlitzer, M. Omidi, L. Ren, S. Kruber, R. Nimer, W. D. Robertson, A. Horst, R. J. D. Miller, and H. Schlüter, Angew. Chem., Int. Ed. Engl. **54**, 285 (2015).
[16]L. Ren, W. D. Robertson, R. Reimer, C. Heinze, C. Schneider, D. Eggert, P. Truschow, N.-O. Hansen, P. Kroetz, J. Zou, and R. J. D. Miller, Nanotechnology **26**, 284001 (2015).
[17]J. Zou, F. Talbot, A. Tata, L. Ermini, K. Franjic, M. Ventura, J. Zheng, H. Ginsberg, M. Post, D. R. Ifa, D. Jaffray, R. J. D. Miller, and A. Zarrine-Afsar, Anal. Chem. **87**, 12071 (2015).
[18]T. E. Itina, L. V. Zhigilei, and B. J. Garrison, J. Phys. Chem. B **106**, 303 (2002).
[19]E. Leveugle and L. V. Zhigilei, J. Appl. Phys. **102**, 074914 (2007).
[20]L. V. Zhigilei, Appl. Phys. A **76**, 339 (2003).
[21]L. V. Zhigilei and B. J. Garrison, J. Appl. Phys. **88**, 1281 (2000).
[22]L. V. Zhigilei, P. B. S. Kodali, and B. J. Garrison, J. Phys. Chem. B **102**, 2845 (1998).
[23]L. V. Zhigilei, E. Leveugle, B. J. Garrison, Y. G. Yingling, and M. I. Zeifman, Chem. Rev. **103**, 321 (2003).
[24]L. V. Zhigilei, Y. G. Yingling, T. E. Itina, T. A. Schoolcraft, and B. J. Garrison, Int. J. Mass Spectrom. **226**, 85 (2003).
[25]R. Knochenmuss and L. V. Zhigilei, J. Mass Spectrom. **45**, 333 (2010).
[26]R. Knochenmuss and L. V. Zhigilei, Anal. Bioanal. Chem. **402**, 2511 (2012).
[27]R. Milo, BioEssays **35**, 1050 (2013).
[28]L. V. Zhigilei, P. B. S. Kodali, and B. J. Garrison, J. Phys. Chem. B **101**, 2028 (1997).
[29]E. A. Colbourn, *Computer Simulation of Polymers* (Longman Scientific & Technical, 1994).
[30]M. Tabetah, A. Matei, C. Constantinescu, N. P. Mortensen, M. Dinescu, J. Schou, and L. V. Zhigilei, J. Phys. Chem. B **118**, 13290 (2014).
[31]R. J. Abraham and R. Stōlevik, Chem. Phys. Lett. **58**, 622 (1978).
[32]P. M. Morse, Phys. Rev. **34**, 57 (1929).
[33]Y. G. Yingling, L. V. Zhigilei, and B. J. Garrison, J. Photochem. Photobiol. A **145**, 173 (2001).
[34]B. Gavish, E. Gratton, and C. J. Hardy, Proc. Natl. Acad. Sci. U. S. A. **80**, 750 (1983).
[35]W. M. Jacobs, D. A. Nicholson, H. Zemer, A. N. Volkov, and L. V. Zhigilei, Phys. Rev. B **86**, 165414 (2012).
[36]D. R. Lide, *CRC Handbook of Chemistry and Physics* (CRC Press, 2003).
[37]J. Gómez, V. J. Hilser, D. Xie, and E. Freire, Proteins **22**, 404 (1995).
[38]D. Kraemer, M. L. Cowan, A. Paarmann, N. Huse, E. T. J. Nibbering, T. Elsaesser, and R. J. D. Miller, Proc. Natl. Acad. Sci. U. S. A. **105**, 437 (2008).
[39]G. T. Ibragimova and R. C. Wade, Biophys. J. **74**, 2906 (1998).
[40]D. Frenkel and B. Smit, *Understanding Molecular Simulation: From Algorithms to Applications*, 2nd ed. (Academic Press, San Diego, 2002).
[41]R. Knochenmuss and L. V. Zhigilei, J. Phys. Chem. B **109**, 22947 (2005).
[42]S. Georgiou, A. Koubenakis, J. Labrakis, and M. Lassithiotaki, Appl. Surf. Sci. **127–129**, 122 (1998).
[43]L. M. Cousins and S. R. Leone, Chem. Phys. Lett. **155**, 162 (1989).